Article

pH Distribution along Growing Fungal Hyphae at Microscale

Bi-Jing Xiong [1], Claire E. Stanley [2] ID, Christian Dusny [3], Dietmar Schlosser [1] ID, Hauke Harms [1]
and Lukas Y. Wick [1],* ID

[1] Helmholtz Centre for Environmental Research-UFZ, Department of Environmental Microbiology,
Permoserstraβe 15, 04318 Leipzig, Germany; bijing.xiong@ufz.de (B.-J.X.); dietmar.schlosser@ufz.de (D.S.);
hauke.harms@ufz.de (H.H.)
[2] Department of Bioengineering, Imperial College of London, South Kensington Campus,
London SW7 2AZ, UK; claire.stanley@imperial.ac.uk
[3] Helmholtz Centre for Environmental Research-UFZ, Department of Solar Materials, Permoserstraβe 15,
04318 Leipzig, Germany; christian.dusny@ufz.de
* Correspondence: lukas.wick@ufz.de; Tel.: +49-341-235-1316

Abstract: Creating unique microenvironments, hyphal surfaces and their surroundings allow for
spatially distinct microbial interactions and functions at the microscale. Using a microfluidic system
and pH-sensitive whole-cell bioreporters (*Synechocystis* sp. PCC6803) attached to hyphae, we spatially
resolved the pH along surfaces of growing hyphae of the basidiomycete *Coprinopsis cinerea*. Time-lapse
microscopy analysis of ratiometric fluorescence signals of >2400 individual bioreporters revealed
an overall pH drop from 6.3 ± 0.4 ($n = 2441$) to 5.0 ± 0.3 ($n = 2497$) within 7 h after pH bioreporter
loading to hyphal surfaces. The pH along hyphal surfaces varied significantly ($p < 0.05$), with pH
at hyphal tips being on average ~0.8 pH units lower than at more mature hyphal parts near the
entrance of the microfluidic observation chamber. Our data represent the first dynamic in vitro
analysis of surface pH along growing hyphae at the micrometre scale. Such knowledge may improve
our understanding of spatial, pH-dependent hyphal processes, such as the degradation of organic
matter or mineral weathering.

Keywords: bioreporter; microfluidics; hyphosphere; mycosphere; *Coprinopsis cinerea*; single cell

1. Introduction

Fungi and bacteria co-inhabit a wide variety of environments. Creating unique and
dynamic microenvironments, hyphal surfaces often allow for spatially distinct microbial
interactions and functions near and/or affected by hyphae. The hyphosphere [1] is a zone
of fungal activity and a favourable habitat [2,3] for bacterial colonisation and dispersal [4–6].
As well as oxygen availability [6,7], pH is an important driver for hyphal-bound microbial
activity [1] such as bacterial motility [8]; degradation of organic matter, lignin and lignocel-
lulose; the mobilisation and transport of nutrients [9,10]; mineral weathering [11]; and soil
structure changes. Fungal mycelia typically modulate the environmental pH in their hypho-
sphere [12,13]. However, knowledge of the microscale pH of dynamically changing hyphal
surfaces still is limited and often inferred only after destructive sampling [11]. pH analysis
techniques involve nanoparticles [14,15], needle-type microelectrodes [16,17] or planar
optodes [9]. Although nanoparticle-based sensors may allow pH profiles to be detected at
the nanoscale, they are not yet commercially available. Despite being fast and non-invasive,
planar optodes have a typical sensing resolution of >150 μm, and hence are not suitable for
resolving pH at scales relevant for cellular functioning [18,19]. Needle-type microelectrodes
with a tip size of ~3 μm [20] have been used to analyse microscale pH in growing hyphae.
They are, however, highly invasive and, since used for mapping or time-lapse monitoring
of pH along hyphae, would require 100 insertions per 1 mm to achieve a resolution of
10 μm. Many fungal mycelia, however, express significant multiscale heterogeneity in their
extensive network and even between adjacent compartments of the same hypha [21], as

has been evidenced by a spatially resolved fungal secretome analysis of *Aspergillus niger* mycelia [22]. Real-time microscale mapping of pH changes along extended mycelia using microelectrodes thus remains challenging. Using a whole-cell bacterial pH bioreporter (*Synechocystis* sp. PCC6803_peripHlu) that allows for spatial and temporal in vitro analysis of environmental pH at the single-cell scale (~3 μm), recent work [12] mapped spatially distinct and temporally stable gradients between pH 4.4 and 5.8 in habitats during hyphal colonisation. The pH bioreporter is based on a periplasm-localised, ratiometric pH-sensitive green fluorescent protein (GFP), pHluorin2, that displays varying bimodal excitation at 395 nm and 475 nm with maximum emission at 510 nm, thus reporting the local environmental pH [12]. By attaching >2400 *Synechocystis* sp. PCC6803 bioreporter cells to hyphal monolayers of the well-characterised saprophytic [23] basidiomycete *Coprinopsis cinerea*, we dynamically mapped the pH on the immediate surface of growing hyphae in a stringently controlled microfluidic system [24]. Time-lapse fluorescence microscopy was performed to examine pH-dependent fluorescence signals of individual bioreporter cells. While our study revealed an overall acidic mycelial surface, a temporally and spatially heterogeneous pH distribution along *C. cinerea* hyphae was demonstrated.

2. Materials and Methods

2.1. Microorganisms, Growth Conditions and Analysis of Water Contact Angles

Synechocystis sp. PCC6803_peripHlu was cultivated in modified blue-green 11 (BG 11) medium, as described before [12]. At the mid-exponential phase (OD_{750} = 2.8), 1 mL was harvested and centrifuged for 5 min at $7000\times$ g at 10 °C, and the supernatant was discarded. The cell pellet was re-suspended in 5 mL of modified BG 11 medium to obtain a suspension of OD_{750} = ~0.05 that was used for further inoculation of the microfluidic devices (as described in Section 2.2.2). *C. cinerea* was used as a well-characterised pH-modifying filamentous fungus [23]. It was cultivated at 25 °C for 3 days on yeast–malt extract–glucose (YMG) medium [24].The water contact angles (θ_w) of the fungus *C. cinerea*, and pH bioreporter *Synechocystis* sp. PCC6803_peripHlu were estimated using a drop size analyser (DSA) 100 system (Krüss GmbH, Hamburg, Germany). Briefly, mycelia of *C. cinerea* were cultivated for 2–3 days on filters with a diameter of 25 mm (0.45 μm, NC 45, Cellulose Nitrate Membrane Whatman, Maidstone, Kent, United Kingdom) placed on the surface of the YBG 11 [12] agar plate. *Synechocystis* sp. PCC6803_peripHlu cells were cultivated in flasks as described above and cell culture with an OD_{750} = 2.8 was placed to the aforementioned filters. Filters covered with either *C. cinerea* mycelia or the pH bioreporter cells were removed from the plate and placed onto filters with a diameter of 5 cm (pore size 0.45 μm) in a filtration unit, and washed three times under suction with 20 mL 10 mM phosphate-buffered saline (PBS), pH 7.2. Afterwards, filters were mounted on a glass slide and air-dried for two hours at room temperature. After that, contact angles were measured as detailed elsewhere [25,26].

2.2. Time-Resolved In Vitro Hyphal Surface pH Sensing

2.2.1. Microfluidic Device

Microfluidic devices (Figure 1a) were prepared as described by Stanley et al. [24]. They were based on a channel architecture (Figure 1b) enabling laminar flow conditions [27] as a result of actively pumping solutions into the observation chamber. The key components of the device included (i) a fungal constriction channel, which limits the number of hyphae entering into the device and prevents backflow; (ii) an observation chamber allowing hyphal development and high-resolution microscopic imaging (i.e., Figure 1c); and (iii) a bacterial inlet (Figure 1b). The observation chamber (l × w: 5000 × 1000 μm) had a channel height of 10 μm to allow the formation of a monolayer of *C. cinerea* hyphae (hyphal diameter: ~7 μm). *Synechocystis* sp. PCC6803_peripHlu cells were introduced into the observation chamber by actively pumping cell solutions via the bacterial inlet (Figure 1b).
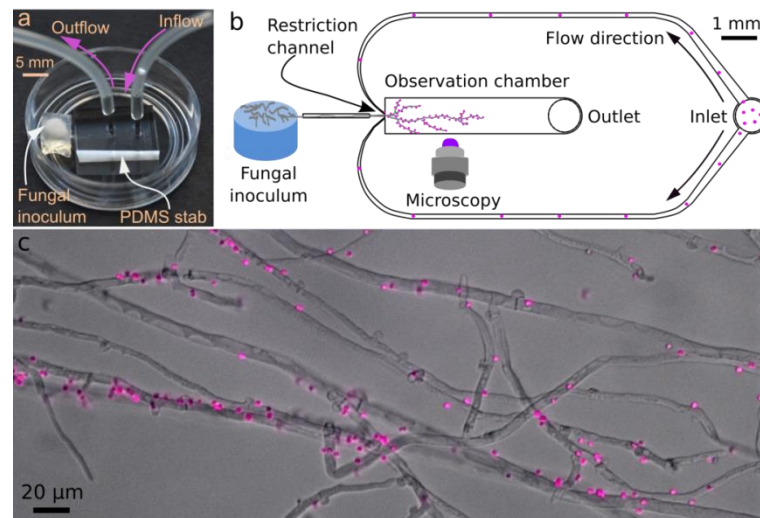
Figure 1. Photograph and schematic of the microcosm for in vitro time-resolved pH monitoring at hyphal surfaces. (**a**) Photograph of the experimental setup consisting of a fungal inoculum placed ca. 1 mm from the lateral opening of the microfluidic device and tubing used to load the bioreporter into to microchannels via the device inlet. (**b**) Schematic of the microcosm depicted in (a) consisting of an agar patch and microchannels embodied in a PDMS stab. The microchannels allow for the development of a hyphal monolayer in the observation chamber and subsequent loading of the pH bioreporters via an inlet and outlet system. (**c**) Micrograph showing typical distribution and attachment of *Synechocystis* sp. PCC6803_peripHlu pH bioreporters (pink dots) along hyphae of *C. cinerea* in the observation chamber.

2.2.2. Microfluidic Device: Fungal Inoculation and Loading of Bioreporters

Using a 1 mL syringe, the microfluidics were filled under sterile conditions with the modified BG 11 (pH 7.2) medium supplemented with 10 mM glucose for *C. cinerea*. Using a scalpel, a squared agarose piece (Ø: 0.5 cm) was cut from the peripheral growth zone of a *C. cinerea* plate. The piece was placed at a distance of ~1 mm from the entrance (Figure 1a,b) and the microcosm was sealed and incubated in the dark at 25 °C. The microcosms were examined regularly by microscopy to detect the time of hyphal arrival (after ca. 20 h of incubation) at the entrance of the observation chamber (denoted in the manuscript as $t = 0$ h). The setup then was incubated for another 18 h at 25 °C to enable the hyphae to cover two-thirds of the observation chamber (ca. 3500 μm, cf. Figure 1b). At $t = 18$ h, the microcosm was opened in a clean bench, and a sterile tubing system connected the inlet and outlet (Figure 1a,b) of the microfluidic. A suspension of pH bioreporter cells (OD$_{750}$ = ~0.05, or 2.74×10^9 cells L^{-1}) was pumped into the observation chamber using a syringe pump (KD, Scientific Inc., North Logan, UT, USA) loaded with Luer-lock syringes (Injekt Solo, 2 mL, B. Braun, Melsungen, Germany) at a volumetric flow rate of 300 μL h^{-1} for 15 min in the clean bench. After that, the tubing system was disconnected and the microcosm sealed. The whole observation chamber was microscopically imaged to record mycelial structures and fluorescence signals of the locally distributed bioreporters on the hyphal surface. Mycelial growth and bioreporter signals were recorded for another seven hours at hourly intervals. The microcosms were kept in the dark when not used for microscopy.

Setups in the absence of a fungal inoculum were used as controls. In controls, a squared sterile agarose piece (Ø: 0.5 cm) was placed at a distance of ~1 mm from the PDMS stab. The subsequent treatment and microscopic monitoring of control microcosms were performed following the same procedure as described above, except the bioreporter loading rate was changed to 100 μL h^{-1} to increase bioreporter retention time in the observation chamber.

2.2.3. Time-Resolved Microscopic Imaging

Ratiometric pHluorin2 expressed by *Synechocystis* sp. PCC6803_peripHlu displays a bimodal excitation at 395 nm and 475 nm with maximum emission at 510 nm [12,28,29].

Upon acidification, emission at 510 nm after excitation at 395 nm ($I_{510\text{-}395}$) decreases, yet increases after excitation at 475 nm ($I_{510\text{-}475}$). The 510 nm emission intensity ratio from two excitations ($R_{I510\text{-}475/I510\text{-}395}$, abbreviated as $R_{I475/I395}$) thus increases in response to decreasing environmental pH. Ratiometric fluorescence signals ($I_{510\text{-}475}$ and $I_{510\text{-}395}$) of individual bioreporter cells were monitored as described before applying minor modifications. Briefly, an automated inverted Zeiss microscope equipped with a Colibri LED fluorescence excitation unit (Axio Observer, Carl Zeiss Microscopy GmbH, Jena, Germany) and a customised fluorescence filter set was used for fluorescence imaging (AHF Analysentechnik AG, Tübingen, Germany). In time-lapse imaging, brightfield images were acquired using LED illumination (exposure time 80 ms, light source intensity 4.7 Volt). Fluorescence images were taken using an emission wavelength of 510 nm after 475 nm excitation (exposure time 100 ms, light source intensity 0.5 V) and 395 nm excitation (exposure time 200 ms, light source intensity 0.5 V). Both brightfield and fluorescence images were taken at hourly intervals. In fluorescence micrographs, red and blue were used as pseudo-colours to represent fluorescence emission excited at 475 nm and 395 nm, respectively. Our micrographs show the overlay of the two emission signals leading to pH-dependent changes of the bioreporter pseudo-colours, i.e., purple cells at pH 7, pink at pH 6 and red at pH 5, as described previously [12]. All microscopic images were taken at a total magnification of 400×, employing an objective lens Plan-Apochromat 40×/1.40 Ph3 M27 (Carl Zeiss Microscopy GmbH, Jena, Germany).

2.3. Image Analysis and Spatial Data Interpretation

The $I_{510\text{-}475}$ and $I_{510\text{-}395}$ of individual bioreporter cells loaded on the hyphal surface were analysed with ImageJ (https://imagej.net, accessed on 30 September 2021) [30], following a previously reported protocol [12]. The $R_{I475/I395}$ of the individual bioreporter cells were calculated and transformed to pH values by using a previously established pH calibration curve ($R_{I475/I395}$ = −0.5012 × (environmental pH) + 4.0386; validating range: pH 4.4 to pH 7.4 [12]). The time-resolved vector data (n > 2400 cells at each of the eight imaging time points) were then interpreted to examine (i) the average surface pH of the hyphae at given time points and (ii) the local surface pH of growing hyphae. The position of individual bioreporter cells is given by the longitudinal (*x*-axis) distance from the entrance of the microfluidic observation chamber (Figure 1b).

3. Statistical Analysis

Statistical analyses were performed using IBM SPSS Statistics software (version 26). The normality of data was verified with the Shapiro–Wilk test. To compare the differences between the two groups (i.e., pH at the hyphal tips and the more mature parts of the fungal mycelium), a *t*-test was used. To compare differences between multiple groups, means were compared using one-way ANOVA followed by either the least significant difference (LSD) test or Dunnett's T3 test, depending on whether equal variances were or were not assumed, respectively.

4. Results

4.1. Time-Resolved Average Hyphal Surface pH

Using the pH-sensitive bioreporter *Synechocystis* sp. PCC6803 (Figure 2), we mapped the pH at the immediate surface of growing *C. cinerea* hyphae hourly (Figure 3) after the appearance of the first hyphal tips in the microfluidic observation chamber (ca. 18–25 h post inoculation, denoted as *t* = 0 h). At *t* = 18 h, the hyphal monolayer extended ~3600 μm into the liquid-filled observation chamber (Figure S1). Then, the pH bioreporter suspension was flushed through the observation chamber to attach the pH bioreporters to the hydrophobic (water contact angle θ_w = 128° ± 2°, Table S1) hyphal surfaces (Figure 2). Only a few non-hyphal-bound cells (n < 50) were counted in the observation chambers. These cells were not included in the analysis of hyphal surface pH. We further observed some hyphal-attached pH bioreporter cells to disperse along *C. cinerea* hyphae via swarming or due to hyphal

elongation (Figure S4, animated gif). This may explain why we also detected bioreporters on newly formed *C. cinerea* hyphae during the incubation (Figure 2b). Despite this redistribution, bioreporter cell numbers remained quasi-stable throughout the experiment (2441 at *t* = 18 h and 2497 cells at *t* = 25 h).
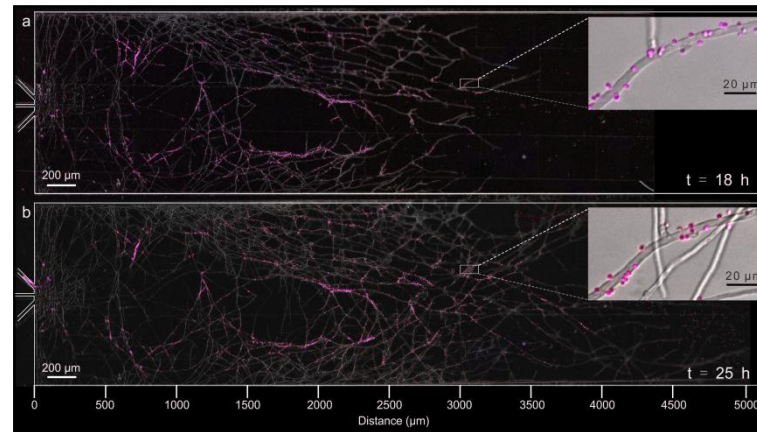
Figure 2. Micrographs depicting hyphal development of *C. cinerea* in the observation chamber and corresponding changes in the pseudo-colours of hyphal-bound *Synechocystis* sp. PCC6803_peripHlu pH bioreporter cells. The pseudo-colours refer to the overlay of two pH-dependent emission signals ($R_{I475/I395}$). (**a**) Hyphal development at *t* = 18 h and most pH bioreporters show a pseudo-colour of magenta (pH ~ 6.3). (**b**) Hyphal development at *t* = 25 h and most pH bioreporters show a pseudo-colour of red (pH ~ 5.0). For better visibility, the contours of microchannels are marked by white lines.
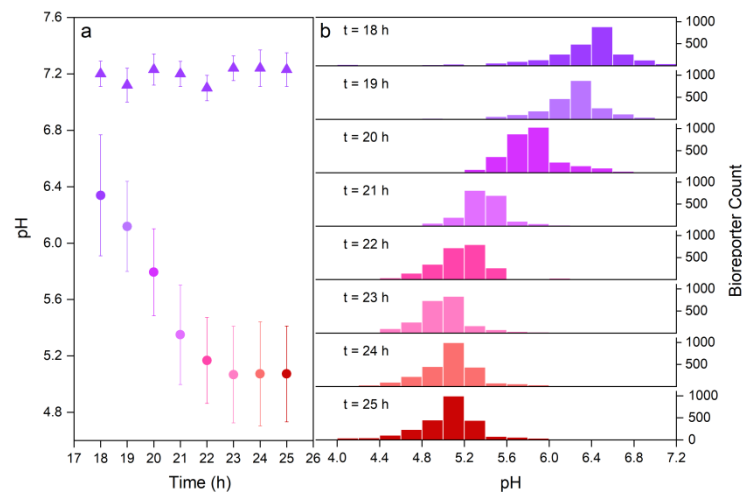

Figure 3. Time-dependent average pH and histogram of pH distribution on hyphal surfaces of *C. cinerea*. The pH was assessed by the hyphal-bound *Synechocystis* sp. PCC6803 bioreporter cells. (**a**) Bioreporter data encompass the average and standard deviation of *n* > 2400 cells (circles, (**a**)). Experiments in the absence of *C. cinerea* served as controls (triangles; *n* > 2200 cells). Time was denoted as *t* = 0 h when the first hyphal tips appeared in the microfluidic observation chamber. The bioreporter cells were loaded to the hyphae at *t* = 18 h of the noted time. (**b**) Corresponding pH distribution on hyphal surfaces of *C. cinerea* at *t* = 18–25 h.

Bioreporters revealed an average hyphal surface pH of 6.3 ± 0.4 at *t* = 18 h (Figure 3a; $R_{I475/I395}$ = 0.88 ± 0.21, *n* > 2400 cells) and a subsequent drop to 5.0 ± 0.3 at *t* = 23 h (Figure 3a; $R_{I475/I395}$ = 1.53 ± 0.14). Thereafter, the average pH remained unchanged up to the end of the experiment (*t* = 25 h, 5.0 ± 0.3, Figure 3a; $R_{I475/I395}$ = 1.53 ± 0.15). The pH reported by the biosensors in fungus-free controls was 7.2 ± 0.1 and remained

stable throughout the observation period (Figure 3a, triangles). Histograms reflecting the time-dependent pH frequency (Figure 3b) revealed substantial pH differences (ΔpH) along mycelia ranging from $\Delta pH_{18-20\,h}$ = 2.0–2.4 at t = 18–20 h and from $\Delta pH_{22-25\,h}$ = ~1.6 at t = 22–25 h, as shown by the wider histogram range at t = 18–20 h compared to those at t = 22–25 h (Figure 3b).

4.2. Distribution of Surface pH along Growing Hyphae

Time-resolved vector data of pH sensed by the biosensors were analysed to examine pH distribution along the direction of hyphal growth (Figure 4). Different surface pH was observed along the growing hyphae at all observation points (Figures 4 and S2). Surface pH at the hyphal tips (Figure 4) was found to be 0.7 (t = 18 h) to 0.9 (t = 25 h) pH units lower than at more mature hyphal areas near the entrance of the microfluidic observation chamber. Histograms of surface pH (Figure S3) at the hyphal tips (i.e., at a 500 µm distance away from the hyphal tips) showed higher pH differences (e.g., ΔpH = 2.9 at t = 18 h) than at the entrance (ΔpH = 0.9 at t = 18 h) of the observation chamber (cf. Figures 4 and S3).
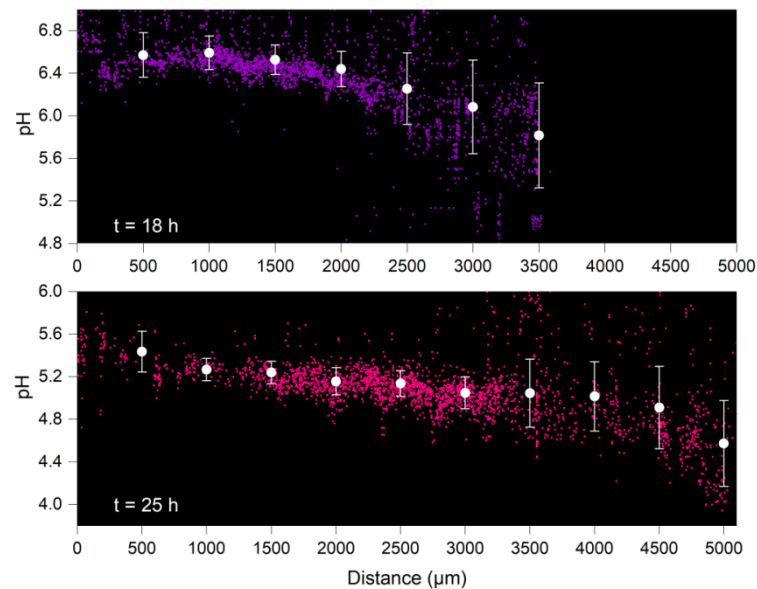
Figure 4. Longitudinal distribution of sensed pH by *Synechocystis* sp. PCC6803 bioreporter cells attached to *C. cinerea* hyphae. Data reflect average pH and pH distribution of n > 2400 cells incubated at various distances along the observation chamber at t = 18 h and t = 25 h. Average data include pH signals from all cells at ±500 µm from given distances. Significantly (p < 0.05) lower pH (≈0.8 pH) was observed near the hyphal tips (cf. at >3000 µm at t = 18 h, and at >4500 µm at t = 25 h) than those at the more mature part at the entrance of the observation chamber (x = 0–500 µm).

5. Discussion

5.1. Time-Resolved In Vitro Analysis of Hyphal Surface pH

By combining a robust single-cell pH bioreporter and microfluidic technology, we developed a novel method allowing for dynamic high-resolution monitoring of spatial hyphal surface pH at micrometre scale. Our data reveal a dynamic spatial pH distribution in the direct vicinity of hyphal surfaces. In contrast to pH = 7.2 in a hypha-free environment (Figure 3a), we observed continuously decreasing average pH values around hyphae that can be ascribed to fungal metabolic activity. The pH approached a value of 5.0 ± 0.3 at t = 23 h. This finding is in line with an earlier study assessing the pH in the area surrounding hyphae of *C. cinerea* by abiotic and whole-cell bioreporter approaches [12], where an overall acid pH (pH 5.0) and temporally stable microscale pH gradients of ~1.4 pH units over distances of ~20 µm were detected in areas surrounded by *C. cinerea* hyphae. Using a microfluidic system to uniformly attach micrometre-sized (Ø: ≈3 µm)

pH reporting *Synechocystis* sp. PCC6803 cells in a spatially specific manner, we report here microscale-sensed pH, i.e., at the immediate surface of growing hyphae.

Many studies report the attachment and biofilm formation of bacteria on fungal hyphae (e.g., [31–33]) as the basis of interactions such as mutualism, commensalism, antagonism or competition for nutrients or oxygen [31,34]. Force interactions and initial attachment of single bacteria [24,35] or other biological entities such as phages [32] to the fungal surface can be suitably described by the DLVO theory of colloidal interaction [36,37]. According to the DLVO approach, particle attachment to hyphal surfaces depends on both the van der Waals attraction (as can be approximated by the hyphal surface hydrophobicity and the water contact angle θ_w) and the electrostatic repulsion between two surfaces in a liquid medium. Bacterial attachment to both hydrophilic and hydrophobic hyphal surfaces is thus to be expected. Here, we successfully loaded $n > 2400$ bioreporter cells to the *C. cinerea* growing hyphal monolayer ($\theta_w = 128° \pm 2°$) in a microfluidic device that allowed for non-invasive dynamic mapping of hyphal-attached bioreporter cells and their pH-sensitive signals (Figures 2 and 3), as well as for the assessment of the assumed multiscale heterogeneity existing in filamentous fungi [21]. In our system, we observed poor attachment of bioreporter cells to the walls of the observation chamber in the presence of *C. cinerea* hyphae. As hyphal activity and bacterial fungal interactions may also depend on microscale gradients forming around hyphae, further development of our system will need to detect both surface pH and pH gradients forming around single hyphae, by developing tailored surfaces of the microfluidic observation chambers allowing for better bioreporter attachment.

5.2. pH on the Hyphal Surface and Its Ecological Significance

The litter decomposing fungus *C. cinerea* [23,38] is a well-characterised [23] lignocellulolytic basidiomycete. Basidiomycetes are known to excrete small organic acids, lowering the environmental pH in order to meet the requirements of their different extracellular enzymes [13,39,40] such as cellulases (optimal pH ~5 [41]), pectinases (optimal pH ~4 [42]) and phenol oxidases (optimal pH 4–5 [43]). In particular, the pH ranges observed in our study (6.3 ± 0.4 to 5.0 ± 0.3, Figure 3) seem to be in accordance with ideal pH levels reported for extracellular enzymes encoded in the *C. cinerea* genome [44,45]. For example, laccases involved in the degradation of lignin [44,45] and the oxidation of phenolic substrates are most active either at acidic (*C. cinerea* Lcc8 [46], optimal pH of 4.5–5.0) or circum-neutral pH (Lcc1 and Lcc9 [47,48], pH 6.5), respectively, whereas the optimal pH is 5–5.5 for lytic polysaccharide monooxygenases (LPMO) cooperating with laccases [49]. For dye decolourising peroxidases, optimal pH values of 3–6 were reported [2]. Although extracellular enzymes have been observed to diffuse a few hundred micrometres away from hyphae [50], many of them have also been found to be retained on the hyphal surface [51]. Thus, a favourable pH range on the hyphal surface may be one of the contributors to the high fungal activity observed close to the hyphal surface [11,52]. Likewise, such spatial and temporal pH traits may be used to dynamically identify the locations of high enzyme activity along hyphal surfaces. Using oxygen-sensitive particles (Ø: 8 μm), a recent study revealed microscale oxygen heterogeneity in the liquid (~10 μm [6]) around air-exposed hyphae of *C. cinerea* [6]. In our study, we observed 0.7–0.9 units lower and more variable pH values at growing tips than at the more mature hyphal parts (Figures 4 and S3), thereby likely being a driver and result of hyphal elongation, as described by the acid growth hypothesis for plant root and filamentous organisms [20,53,54]. The acid growth hypothesis postulates that plant or fungal phytotoxin fusicoccin and plant hormone Indole-3-acetic acid can induce proton secretion concomitant with the induction of apical elongation by rapid acidification of the thick extension-limiting cell wall [55,56].

Although pH is known to be a major driver for microbial community structure [57,58], it remains mainly elusive as to whether, and to what degree, varying hyphal surface pH may influence the bacterial dispersal and/or the (uneven) colonisation of hyphae [59]. Hence, knowledge of dynamic pH distributions along mycelia could form an important

next step in the examination of pH-mediated microniche differentiation on the hyphal surfaces in microbiome-on-a-chip [60] studies. As bacterial (flagellar) motility is known to be affected by the environmental conditions, e.g., the local pH [8,61–63], variations in hyphal surface pH may modulate bacterial swimming behaviour, and thereby influence bacterial transport along hyphal networks, and bacterial colonisation of and functioning in new habitats [5,64]. Spatially resolved microscale pH analysis with single-hypha resolution thus also enables a better understanding of bacterial fungal interactions and, hence, their roles in driving ecosystems services and functioning at the macroscale.

Supplementary Materials: The following supporting information can be downloaded at: https://www.mdpi.com/article/10.3390/jof8060599/s1, Figure S1: Inverted brightfield micrograph of *Coprinopsis cinerea* hyphal monolayer in the observation chamber before loading of pH bioreporter cells to the microfluidic system. For better visibility of *C. cinerea* hyphae, contrast and brightness of the micrograph were adjusted using ImageJ; Figure S2: Longitudinal distribution of pH sensed by *Synechocystis* sp. PCC6803 bioreporter cells attached to *C. cinerea* hyphae. The *x*-axis reflects the distance from the entrance to the observation chamber, i.e., where the hyphal tips first enter. pH bioreporter cells reflect a temporally changing and longitudinal pH gradient ($\approx$0.8 pH) along the growing *C. cinerea* hyphae; Figure S3: Histogram of distribution of surface pH of (more mature) hyphae near the entrance of the observation chamber and at the hyphal tips of *C. cinerea.* (a) pH distribution on hyphal surfaces at 0–500 μm from the start of the observation chamber at $t = 18$ and 25 h, resp. (b) pH distribution on hyphal surfaces at a distance 500 μm away from the hyphal tips at $t = 18$ and 25 h, resp; Figure S4: Movement and dispersal of pH bioreporter *Synechocystis* sp. PCC6803_periHlu cells along *C. cinerea* hyphae; Table S1: Water contact angles of mycelial surfaces of *Coprinopsis cinerea* and *Synechocystis* pH bioreporter cells.

Author Contributions: B.-J.X. and L.Y.W. designed the study. B.-J.X. performed the experiments. B.-J.X., L.Y.W., C.E.S., C.D., D.S. and H.H. wrote the manuscript. All authors have read and agreed to the published version of the manuscript.

Institutional Review Board Statement: Not applicable.

Informed Consent Statement: Not applicable.

Data Availability Statement: The data presented in this study are available on request from the authors.

Conflicts of Interest: The authors declare no conflict of interest.

References

1. Worrich, A.; Wick, L.Y.; Banitz, T. Ecology of contaminant biotransformation in the mycosphere: Role of transport processes. *Adv. Appl. Microbiol.* **2018**, *104*, 93–133. [PubMed]
2. Liers, C.; Aranda, E.; Strittmatter, E.; Piontek, K.; Plattner, D.A.; Zorn, H.; Ullrich, R.; Hofrichter, M. Phenol oxidation by DyP-type peroxidases in comparison to fungal and plant peroxidases. *J. Mol. Catal. B Enzym.* **2014**, *103*, 41–46. [CrossRef]
3. Boer, W.d.; Folman, L.B.; Summerbell, R.C.; Boddy, L. Living in a fungal world: Impact of fungi on soil bacterial niche development. *FEMS Microbiol. Rev.* **2005**, *29*, 795–811. [CrossRef]
4. Kohlmeier, S.; Smits, T.H.M.; Ford, R.M.; Keel, C.; Harms, H.; Wick, L.Y. Taking the Fungal Highway: Mobilization of Pollutant-Degrading Bacteria by Fungi. *Environ. Sci. Technol.* **2005**, *39*, 4640–4646. [CrossRef] [PubMed]
5. You, X.; Kallies, R.; Kühn, I.; Schmidt, M.; Harms, H.; Chatzinotas, A.; Wick, L.Y. Phage co-transport with hyphal-riding bacteria fuels bacterial invasion in a water-unsaturated microbial model system. *ISME J.* **2021**, *16*, 1275–1283. [CrossRef] [PubMed]
6. Xiong, B.-J.; Kleinsteuber, S.; Sträuber, H.; Dusny, C.; Harms, H.; Wick, L.Y. Impact of fungal hyphae on growth and dispersal of obligate anaerobic bacteria in aerated habitats. *bioRxiv* **2022**. [CrossRef] [PubMed]

7. Fox, E.; Cowley, E.; Nobile, C.; Hartooni, N.; Newman, D.; Johnson, A. Anaerobic bacteria grow within *Candida albicans* biofilms and induce biofilm formation in suspension cultures. *Curr. Biol.* **2014**, *24*, 2411–2416. [CrossRef]

8. Minamino, T.; Imae, Y.; Oosawa, F.; Kobayashi, Y.; Oosawa, K. Effect of intracellular pH on rotational speed of bacterial flagellar motors. *J. Bacteriol.* **2003**, *185*, 1190–1194. [CrossRef]

9. Kim, M.; Or, D. Microscale pH variations during drying of soils and desert biocrusts affect HONO and NH_3 emissions. *Nat. Commun.* **2019**, *10*, 3944. [CrossRef] [PubMed]

10. Gadd, G.M.; Rhee, Y.J.; Stephenson, K.; Wei, Z. Geomycology: Metals, actinides and biominerals. *Environ. Microbiol. Rep.* **2012**, *4*, 270–296. [CrossRef] [PubMed]

11. Schmalenberger, A.; Duran, A.; Bray, A.W.; Bridge, J.; Bonneville, S.; Benning, L.G.; Romero-Gonzalez, M.E.; Leake, J.R.; Banwart, S.A. Oxalate secretion by ectomycorrhizal Paxillus involutus is mineral-specific and controls calcium weathering from minerals. *Sci. Rep.* **2015**, *5*, 12187. [CrossRef] [PubMed]

12. Xiong, B.-J.; Dusny, C.; Wang, L.; Appel, J.; Lindstaedt, K.; Schlosser, D.; Harms, H.; Wick, L.Y. Illuminate the hidden: In vivo mapping of microscale pH in the mycosphere using a novel whole-cell biosensor. *ISME Commun.* **2021**, *1*, 75. [CrossRef]

13. Hyde, S.M.; Wood, P.M.J.M. A mechanism for production of hydroxyl radicals by the brown-rot fungus Coniophora puteana: Fe (III) reduction by cellobiose dehydrogenase and Fe (II) oxidation at a distance from the hyphae. *Microbiology* **1997**, *143*, 259–266. [CrossRef] [PubMed]

14. Wang, X.d.; Meier, R.J.; Wolfbeis, O.S. Fluorescent pH-sensitive nanoparticles in an agarose matrix for imaging of bacterial growth and metabolism. *Angew. Chem. Int. Ed.* **2013**, *52*, 406–409. [CrossRef] [PubMed]

15. Wencel, D.; Abel, T.; McDonagh, C. Optical chemical pH sensors. *Anal. Chem.* **2014**, *86*, 15–29. [CrossRef]

16. Marzocchi, U.; Bonaglia, S.; van de Velde, S.; Hall, P.O.; Schramm, A.; Risgaard-Petersen, N.; Meysman, F.J. Transient bottom water oxygenation creates a niche for cable bacteria in long-term anoxic sediments of the Eastern Gotland Basin. *Environ. Microbiol.* **2018**, *20*, 3031–3041. [CrossRef] [PubMed]

17. Agethen, S.; Sander, M.; Waldemer, C.; Knorr, K.-H. Plant rhizosphere oxidation reduces methane production and emission in rewetted peatlands. *Soil Biol. Biochem.* **2018**, *125*, 125–135. [CrossRef]

18. Dal Co, A.; Van Vliet, S.; Ackermann, M. Emergent microscale gradients give rise to metabolic cross-feeding and antibiotic tolerance in clonal bacterial populations. *Philos. Trans. R. Soc. B* **2019**, *374*, 20190080. [CrossRef] [PubMed]

19. Rendler, T.; Neburkova, J.; Zemek, O.; Kotek, J.; Zappe, A.; Chu, Z.; Cigler, P.; Wrachtrup, J. Optical imaging of localized chemical events using programmable diamond quantum nanosensors. *Nat. Commun.* **2017**, *8*, 14701. [CrossRef] [PubMed]

20. Neil, A.G.; Darryl, L.K.; Franklin, M.H. Growing hyphae of Achlya bisexualis generate a longtitudinal pH gradient in the surrounding medium. *Microbiology* **1984**, *130*, 2967–2974.

21. Zacchetti, B.; Wösten, H.A.; Claessen, D. Multiscale heterogeneity in filamentous microbes. *Biotechnol. Adv.* **2018**, *36*, 2138–2149. [CrossRef]

22. Krijgsheld, P.; Altelaar, A.M.; Post, H.; Ringrose, J.H.; Müller, W.H.; Heck, A.J.; Wösten, H.A. Spatially resolving the secretome within the mycelium of the cell factory Aspergillus niger. *J. Proteome Res.* **2012**, *11*, 2807–2818. [CrossRef] [PubMed]

23. Stajich, J.E.; Wilke, S.K.; Ahrén, D.; Au, C.H.; Birren, B.W.; Borodovsky, M.; Burns, C.; Canbäck, B.; Casselton, L.A.; Cheng, C. Insights into evolution of multicellular fungi from the assembled chromosomes of the mushroom *Coprinopsis cinerea* (*Coprinus cinereus*). *Proc. Natl. Acad. Sci. USA* **2010**, *107*, 11889–11894. [CrossRef] [PubMed]

24. Stanley, C.E.; Stöckli, M.; van Swaay, D.; Sabotič, J.; Kallio, P.T.; Künzler, M.; deMello, A.J.; Aebi, M. Probing bacterial–fungal interactions at the single cell level. *Integr. Biol.* **2014**, *6*, 935–945. [CrossRef]

25. Smits, T.H.; Wick, L.Y.; Harms, H.; Keel, C. Characterization of the surface hydrophobicity of filamentous fungi. *Environ. Microbiol.* **2003**, *5*, 85–91. [CrossRef]

26. Smits, M.M.; Herrmann, A.M.; Duane, M.; Duckworth, O.W.; Bonneville, S.; Benning, L.G.; Lundström, U. The fungal–mineral interface: Challenges and considerations of micro-analytical developments. *Fungal Biol. Rev.* **2009**, *23*, 122–131. [CrossRef]

27. Stanley, C.E.; Shrivastava, J.; Brugman, R.; Heinzelmann, E.; van Swaay, D.; Grossmann, G. Dual-flow-RootChip reveals local adaptations of roots towards environmental asymmetry at the physiological and genetic levels. *New Phytol.* **2018**, *217*, 1357–1369. [CrossRef]

28. Miesenböck, G.; De Angelis, D.A.; Rothman, J.E. Visualizing secretion and synaptic transmission with pH-sensitive green fluorescent proteins. *Nature* **1998**, *394*, 192–195. [CrossRef] [PubMed]

29. Mahon, M.J. pHluorin2: An enhanced, ratiometric, pH-sensitive green florescent protein. *Adv. Biosci. Biotechnol.* **2011**, *2*, 132. [CrossRef] [PubMed]

30. Schneider, C.A.; Rasband, W.S.; Eliceiri, K.W. NIH Image to ImageJ: 25 years of image analysis. *Nat. Methods* **2012**, *9*, 671–675. [CrossRef] [PubMed]

31. Benoit, I.; van den Esker, M.H.; Patyshakuliyeva, A.; Mattern, D.J.; Blei, F.; Zhou, M.; Dijksterhuis, J.; Brakhage, A.A.; Kuipers, O.P.; de Vries, R.P. *Bacillus acillus* subtilis attachment to *Aspergillus spergillus* niger hyphae results in mutually altered metabolism. *Environ. Microbiol.* **2015**, *17*, 2099–2113. [CrossRef] [PubMed]

32. Ghanem, N.; Stanley, C.E.; Harms, H.; Chatzinotas, A.; Wick, L.Y. Mycelial effects on phage retention during transport in a microfluidic platform. *Environ. Sci. Technol.* **2019**, *53*, 11755–11763. [CrossRef] [PubMed]

33. Miquel Guennoc, C.; Rose, C.; Labbé, J.; Deveau, A. Bacterial biofilm formation on the hyphae of ectomycorrhizal fungi: A widespread ability under controls? *FEMS Microbiol. Ecol.* **2018**, *94*, fiy093. [CrossRef] [PubMed]

34. Deveau, A.; Bonito, G.; Uehling, J.; Paoletti, M.; Becker, M.; Bindschedler, S.; Hacquard, S.; Herve, V.; Labbe, J.; Lastovetsky, O.A. Bacterial–fungal interactions: Ecology, mechanisms and challenges. *FEMS Microbiol. Rev.* **2018**, *42*, 335–352. [CrossRef]

35. Toljander, J.F.; Artursson, V.; Paul, L.R.; Jansson, J.K.; Finlay, R.D. Attachment of different soil bacteria to arbuscular mycorrhizal fungal extraradical hyphae is determined by hyphal vitality and fungal species. *FEMS Microbiol. Lett.* **2006**, *254*, 34–40. [CrossRef]

36. Hermansson, M. The DLVO theory in microbial adhesion. *Colloids Surf. B Biointerfaces* **1999**, *14*, 105–119. [CrossRef]

37. Chrysikopoulos, C.V.; Syngouna, V.I. Attachment of bacteriophages MS2 and ΦX174 onto kaolinite and montmorillonite: Extended-DLVO interactions. *Colloids Surf. B Biointerfaces* **2012**, *92*, 74–83. [CrossRef]

38. Zhang, W.; Wu, S.; Cai, L.; Liu, X.; Wu, H.; Xin, F.; Zhang, M.; Jiang, M. Improved treatment and utilization of rice straw by *Coprinopsis cinerea*. *Appl. Biochem. Biotechnol.* **2018**, *184*, 616–629. [CrossRef]

39. Liaud, N.; Giniés, C.; Navarro, D.; Fabre, N.; Crapart, S.; Gimbert, I.H.; Levasseur, A.; Raouche, S.; Sigoillot, J.-C. Exploring fungal biodiversity: Organic acid production by 66 strains of filamentous fungi. *Fungal Biol. Biotechnol.* **2014**, *1*, 1. [CrossRef]

40. Mäkelä, M.R.; Hildén, K.; Lundell, T.K. Oxalate decarboxylase: Biotechnological update and prevalence of the enzyme in filamentous fungi. *Appl. Microbiol. Biotechnol.* **2010**, *87*, 801–814. [CrossRef]

41. Jahangeer, S.; Khan, N.; Jahangeer, S.; Sohail, M.; Shahzad, S.; Ahmad, A.; Khan, S.A. Screening and characterization of fungal cellulases isolated from the native environmental source. *Pak. J. Bot.* **2005**, *37*, 739.

42. Gummadi, S.N.; Panda, T. Purification and biochemical properties of microbial pectinases—A review. *Process Biochem.* **2003**, *38*, 987–996. [CrossRef]

43. Sinsabaugh, R.L. Phenol oxidase, peroxidase and organic matter dynamics of soil. *Soil Biol. Biochem.* **2010**, *42*, 391–404. [CrossRef]

44. Kilaru, S.; Hoegger, P.J.; Kües, U. The laccase multi-gene family in *Coprinopsis cinerea* has seventeen different members that divide into two distinct subfamilies. *Curr. Genet.* **2006**, *50*, 45–60. [CrossRef] [PubMed]

45. Floudas, D.; Bentzer, J.; Ahrén, D.; Johansson, T.; Persson, P.; Tunlid, A. Uncovering the hidden diversity of litter-decomposition mechanisms in mushroom-forming fungi. *ISME J.* **2020**, *14*, 2046–2059. [CrossRef] [PubMed]

46. Schulze, M.; Geisler, L.; Majcherczyk, A.; Rühl, M. Signal peptide replacement resulted in recombinant homologous expression of laccase Lcc8 in *Coprinopsis cinerea*. *AMB Express* **2019**, *9*, 36. [CrossRef]

47. Schneider, P.; Caspersen, M.B.; Mondorf, K.; Halkier, T.; Skov, L.K.; Østergaard, P.R.; Brown, K.M.; Brown, S.H.; Xu, F. Characterization of a *Coprinus cinereus* laccase. *Enzym. Microb. Technol.* **1999**, *25*, 502–508. [CrossRef]

48. Pan, K.; Zhao, N.; Yin, Q.; Zhang, T.; Xu, X.; Fang, W.; Hong, Y.; Fang, Z.; Xiao, Y. Induction of a laccase Lcc9 from *Coprinopsis cinerea* by fungal coculture and its application on indigo dye decolorization. *Bioresour. Technol.* **2014**, *162*, 45–52. [CrossRef]

49. Brenelli, L.; Squina, F.M.; Felby, C.; Cannella, D. Laccase-derived lignin compounds boost cellulose oxidative enzymes AA9. *Biotechnol. Biofuels* **2018**, *11*, 10. [CrossRef]

50. Houtman, C.J.; Kitin, P.; Houtman, J.C.; Hammel, K.E.; Hunt, C.G. Acridine orange indicates early oxidation of wood cell walls by fungi. *PLoS ONE* **2016**, *11*, e0159715. [CrossRef]

51. Weber, R.; Pitt, D. Filamentous fungi—Growth and physiology. *Appl. Mycol. Biotechnol.* **2001**, *1*, 13–54.

52. Li, X.L.; George, E.; Marschner, H. Phosphorus depletion and pH decrease at the root–soil and hyphae–soil interfaces of VA mycorrhizal white clover fertilized with ammonium. *New Phytol.* **1991**, *119*, 397–404. [CrossRef]

53. Roncal, T.; Ugalde, U.; Irastorza, A. Calcium-induced conidiation in Penicillium cyclopium: Calcium triggers cytosolic alkalinization at the hyphal tip. *J. Bacteriol.* **1993**, *175*, 879–886. [CrossRef] [PubMed]

54. Bittisnich, D.; Williamson, R. Tip-localised H+-fluxes and the applicability of the acid-growth hypothesis to tip-growing cells: Control of chloronemal extension in Funaria hygrometrica by auxin and light. *Planta* **1989**, *178*, 96–102. [CrossRef]

55. Kutschera, U. The current status of the acid-growth hypothesis. *New Phytol.* **1994**, *126*, 549–569. [CrossRef]

56. Marre, E. Fusicoccin: A tool in plant physiology. *Annu. Rev. Plant Physiol.* **1979**, *30*, 273–288. [CrossRef]

57. Lauber, C.L.; Hamady, M.; Knight, R.; Fierer, N. Pyrosequencing-based assessment of soil pH as a predictor of soil bacterial community structure at the continental scale. *Appl. Environ. Microbiol.* **2009**, *75*, 5111–5120. [CrossRef] [PubMed]

58. Tripathi, B.M.; Stegen, J.C.; Kim, M.; Dong, K.; Adams, J.M.; Lee, Y.K. Soil pH mediates the balance between stochastic and deterministic assembly of bacteria. *ISME J.* **2018**, *12*, 1072–1083. [CrossRef] [PubMed]

59. Leveau, J.H.; Preston, G.M. Bacterial mycophagy: Definition and diagnosis of a unique bacterial–fungal interaction. *New Phytol.* **2008**, *177*, 859–876. [CrossRef]

60. Stanley, C.E.; van der Heijden, M.G. Microbiome-on-a-chip: New frontiers in plant–microbiota research. *Trends Microbiol.* **2017**, *25*, 610–613. [CrossRef]

61. Yang, P.; Oliveira da Rocha Calixto, R.; van Elsas, J.D. Migration of Paraburkholderia terrae BS001 along old fungal hyphae in soil at various pH levels. *Microb. Ecol.* **2018**, *76*, 443–452. [CrossRef] [PubMed]

62. Yang, P.; Zhang, M.; van Elsas, J.D. Role of flagella and type four pili in the co-migration of Burkholderia terrae BS001 with fungal hyphae through soil. *Sci. Rep.* **2017**, *7*, 2997. [CrossRef] [PubMed]

63. Blair, D.F. Flagellar movement driven by proton translocation. *FEBS Lett.* **2003**, *545*, 86–95. [CrossRef]

64. Simon, A.; Bindschedler, S.; Job, D.; Wick, L.Y.; Filippidou, S.; Kooli, W.M.; Verrecchia, E.P.; Junier, P. Exploiting the fungal highway: Development of a novel tool for the in situ isolation of bacteria migrating along fungal mycelium. *FEMS Microbiol. Ecol.* **2015**, *91*, fiv116. [CrossRef] [PubMed]